2021

Consistent spring network representation of emphysematous lung from CT images

BOSTON UNIVERSITY

COLLEGE OF ENGINEERING

Thesis

CONSISTENT SPRING NETWORK REPRESENTATION OF EMPHYSEMATOUS LUNG FROM CT IMAGES

by

ZIWEN YUAN

B.S., Boston University, 2019

Submitted in partial fulfillment of the

requirements for the degree of

Master of Science

2021

Approved by

First Reader _____

Béla Suki, Ph.D.
Professor of Biomedical Engineering
Professor of Materials Science and Engineering

Second Reader _____

Kenneth R. Lutchen, Ph.D.
Dean of the College of Engineering
Professor of Biomedical Engineering

Third Reader _____

Jacob Herrmann, Ph.D.
Postdoctoral Associate of Biomedical Engineering

DEDICATION

I would like to dedicate this work to my parents and my grandmother, who supported me with all of their love in the past 24 years. Also, I'm transmitting the same amount of love to my sister and hope she will embrace a better life for every single day since now.

ACKNOWLEDGMENTS

Sincere thanks to my mentor, Prof. Suki, for his infinite patience and incredible help during the past year. He is the first person guiding me in the research area and I cannot express my appreciation to him for the opportunities and the careful leading. He changed my way of thinking about the world as well as the role of myself should play in the world. I am not a good student but he put significant amount of time and patience in leading me to a better me. All the experience that I had the luck to share with him will be branded in my memory for the rest of my life.

The same amount of gratitude to Jake, who put enormous time in helping me solve practical problems hand by hand and leading me to scientifically think the next problem. He is only a few years elder than me but his wisdom, experience and enthusiasm in research is admiring to me and affected me positively in conducting my own project. He has been a goal for me and will encourage me in the future study, work and life.

Special thanks to Dean Lutchen, who take enormous time in discussing my project and gave quite a lot of constructive suggestions, which significantly guided the direction of the thesis. Not only in the project, his idea of "societal engineer" further shaped my idea about my future and what kind of person I should become with all knowledge obtained in Boston University.

To my lab members: Dr. Elizabeth, Jae, Samhita and Kevin, sincere appreciation for your time and concern on me and my project. The existence of you made another home for me in Boston.

CONSISTENT SPRING NETWORK REPRESENTATION OF EMPHYSEMATOUS LUNG FROM CT IMAGES

ZIWEN YUAN

ABSTRACT

Emphysema is a progressive disease characterized by irreversible tissue destruction and airspace enlargement, which manifest as low attenuation area (LAA) on CT images. Previous studies have shown that inflammation, protease imbalance, extracellular matrix remodeling and mechanical forces are collectively playing a role in the progression of emphysema. Elastic spring network models have been applied to investigate the pathogenesis of emphysema from the mechanical perspective. However, all existing models include random removal of springs to mimic the initial locations of LAA clusters from which emphysema progression is initiated. This approach is generically lacking patient specificity of CT scans that precisely reflect the location of LAA in an emphysematous lung. The aim of this work is to develop a novel approach that provides an optimal spring network representation of emphysematous lungs based on apparent density in CT images. The results suggest that the personalized elastic spring network can be used to predict the propagation of structural destruction during emphysema progression. Thus, our approach has the potential to predict disease progression that should be verified by clinical data.

TABLE OF CONTENTS

LIST OF TABLES

LIST OF FIGURES

1 INTRODUCTION

1.1 Background

1.1.1 Force Based Theory for Emphysematous Progression

Emphysema is defined as a condition of lung characterized by abnormal and irreversible enlargement of air spaces distal to terminal bronchioles [6]. The underlying mechanism that drives the pathogenesis and progression of emphysema has not been fully revealed, but a widely accepted mechanism of tissue deterioration is the enzymatic degradation of elastin caused by the imbalance between proteases and anti-proteases [6]. Various proteases have been reported to be capable of inducing emphysema, including neutrophil elastase with α1-antitrypsin deficiency [7] and macrophage elastase after chronic cigarette smoke [8]. In addition, biochemical pathways not involving elastin can also lead to emphysema, like experimental emphysema caused by overexpressing of collagenase [9] and elevated expression of matrix-degrading enzymes [10]. The biochemical pathways leading to emphysema are abundant and they contribute to the pathogenesis collectively. Therefore, no effective target has been identified that could halt the progression of the disease [11].

The lung is under a pre-stressed condition and undergoes cyclic changes of mechanical stress due to breathing. Thus, it is possible that mechanical forces play role in the rupture of alveolar walls during the progression of emphysema [4]. In fact, the contribution of mechanical force to emphysema progression has been advocated for decades [18]. There are also abundant clinical observations supporting the impact of mechanical forces on the progression of emphysema. For example, following lung

volume reduction surgery (LVRS), increased mechanical forces are redistributed to the remaining lung tissue, consistent with the fact that patients with advance emphysema undergo accelerated decline of lung function after LVRS [12].

Since collagen is the most abundant and essential fiber constituting the extracellular matrix serving as a substantial component of connective tissue that supports parenchyma, the breakdown of alveolar wall must involve the breaking of collagen fibers [14]. Normal collagen has high stiffness and failure threshold to protect the lung from rupture at high lung volumes [4], but in the emphysematous lung, collagen is damaged or weakened by various matrix metalloproteinases (MMPs), including alveolar macrophage-derived MMP-1, neutrophil collagenase (MMP-8) and collagenase-3 (MMP-13) [13], or by abnormal remodeling of collagen after damage [14]. Therefore, mechanical force-based modeling approaches implicitly hypothesize that inflammation induces biochemical pathways resulting in the imbalance between enzymes and their inhibitors, leading to an enhanced degradation of the extracellular matrix (ECM) [4]. Following enzymatic and chemical injury, the remodeling of ECM results in weakened and defective collagen fibers with reduced rupture threshold. The decreased failure threshold of alveolar walls allows mechanical stresses during normal breathing to rupture the walls which promotes the progression of emphysema. Since rupture transfers loads to the surrounding fibers and walls, these walls become at risk of rupture. The progression of emphysema then results from the repeated feedback cycle of rupture, redistribution of stresses followed by new ruptures [4]. A linear elastic spring network [3] was applied to show that the mechanical force-based hypothesis of tissue destruction produces a power

law distribution of LAA size that is consistent with CT data, while the biochemical pathogenesis hypothesis produces a near uniform distribution of LAA [4].

1.1.2 Elastic Spring Network Model

Ever since an elastic spring network was introduced to simulate the microscopic structure of emphysematous lung and obtained consistent results with CT images [3], it became a popular and reliable approach to investigate emphysema. The network model was used to study the structure-function relations in emphysematous lung and revealed that lung compliance is sensitive to the change of structural heterogeneity, consistent with experimental results from rat models [29]; the network model helped uncover the role of proteoglycans in stabilizing the alveolar wall and suggest potential treatment for slowing down the progression of emphysema [19]; The network was also applied to predict the structure-function relation in emphysematous lung after LVRS/bLVR and uncovered the relationship between LVRS efficacy and microscopic environmental structure of lung [20]. Thus, the application of spring network models substantially improved our understanding about emphysema and has provided unique insights into the roles of mechanical force in the pathogenesis of emphysema, despite the limitations imposed by the 2D nature of the modeling.

These modeling approaches are also limited in that they can only predict disease progression in a generic sense. The overall goal of this thesis is to extend the existing network models to describe tissue destruction in emphysema on a personalized basis.

1.2 Rationales

Elastic spring networks have been applied previously to study the pathogenesis of emphysema from the biomechanical perspective, contributing to findings consistent with clinical results. CT has become a powerful tool to study emphysema due to its ability to not only provide information on overall lung deterioration, but also precisely indicate the local tissue destruction. Despite the fact that elastic spring networks were applied to interpret the quantitative findings in CT images, most spring networks were simulated independent of actual CT images. Given that lung CT images represent the structure of the lung while spring networks can mimic the microscopic mechanics, this thesis is aimed at introducing a method to personalize an elastic spring network that enables the patient specific prediction of emphysematous progression, which can be beneficial in investigating the underlying mechanism of emphysema, guiding for early intervention and even assisting in surgical and bronchoscopic lung volume reduction treatment.

The elastic spring network approach simulating the coalescence of LAA clusters in an emphysematous lung provides reasonable insights into the role mechanical forces play in the pathogenesis of emphysema [3], and subsequent studies adopted the same method revealing that the progression of emphysema is potentially a complex and collective phenomenon driven by inflammation, protease activity, ECM remodeling and mechanical forces [4]. In a considerable number of cases, the results of the independently initiated elastic spring network were indirectly validated by clinical CT images with specific quantitative indexes, such as %LAA and the exponent D of the power law distribution of LAA sizes. The consistency in those quantitative indexes between the

network model and clinical data reflects that the force-based theory of emphysema progression is reasonable. However, the lack of patient specificity hinders not only the clinical application of the network model but also deeper investigation into the force-driven theory with massively available CT data. Therefore, a reliable method of reconstructing elastic spring networks from lung CT scans must be developed to achieve the personalization of the network model.

Furthermore, a patient-specific Finite Element model (FEM) constructed from CT data has been proposed to predict the results of scoliosis surgery, achieving an excellent consistency with the clinically collected data [21]. The FEM was therefore repeated with 6 more patients and it performed stably for more than half of the cases [22]. The personalization of scoliosis model confirms the viability of the methodology of personalizing FEM from CT data. Furthermore, a non-patient-specific network model has been applied to study the structure-function relation in emphysematous lung after LVRS/bLVR and obtained reasonable results consistent with clinical observation [23]. Thus, the personalization of the network model is necessary to exploit the potential for providing optimal surgical targets by predicting and minimizing the post-surgery deterioration of lung function.

1.3 Objectives

The primary goal of this thesis is to develop a method capable of consistently mapping the characteristic emphysematous lung structure on a CT scan to a hexagonal elastic spring network and predict the progression of the disease on a personalized basis. To achieve this, we set up the following aims:

1) Optimize a technique for mapping individual low attenuation areas (LAAs). Individual LAAs will be mapped onto a hexagonal spring network so as to mimic the microscopic structure of the lung in lung CT scans. Two methods will be used, the first being a naïve approach that simply maps an LAA to the network by eliminating the springs corresponding to the region inside the LAA, and then solves the spring network for mechanical equilibrium. The second approach will first modify the boundary of the LAA before eliminating springs inside the modified boundary, in an attempt to compensate for the distortions of the original LAA boundary that occur after solving the elastic spring network. We will compare the two mapping methods using simplified scenarios, in which the distortion of synthetic LAAs generated during the mapping process will be recorded and analyzed to optimize the mapping technique.

2) Apply LAA mapping techniques to medical image data. Patient CT images containing multiple LAAs of various sizes and shapes will be mapped onto the spring networks using both mapping algorithms from Aim 1. The corresponding spring networks will then be converted back to reconstructed LAAs and compared to the original LAAs. Reconstruction accuracy for individual LAAs will be assessed by the error in %LAA between the original CT and reconstructed apparent CT. The goal is to

find the optimal parameters of the new method that minimize the error.

3) Compare the prediction of the progression of emphysema with the naïve and the proposed methods. The progression of emphysema will be predicted using both mapping approaches. For each mapping method, a series of spring networks will be obtained by iterative degradation, and all networks will be converted into apparent CT images by averaging local spring stiffness. To validate the method, apparent CT images, at similar total %LAA level, from different methods will be compared and the main outcome will be an index measuring the average local structural difference. Furthermore, the largest LAA clusters will be traced in the networks from both mapping methods. The proposed mapping method is expected to generate a spring network with better conserved LAA structures compared with the naïve method, and the difference between predictions is potentially magnified after iterative degradation.

2 METHODS

2.1 The Naïve Mapping

To generate an elastic spring network corresponding to a lung CT image, first LAA clusters are created by thresholding the CT image at -960 HU, which has been validated as the most acceptable threshold for density-based quantification of emphysema [15]. Next, a LAA cluster is selected and a mask of the cluster is created. In the naïve method, the mask image is placed on a pre-stressed linearly elastic hexagonal spring network, in which the rest length of a spring is half of the initial length to generate a pre-stress, and springs inside the mask are eliminated, subsequently creating void area along with the redistribution of stress. The cutting of springs mimics the rupture of the lung parenchyma during the progression of emphysema. Following cutting, the equilibrium configuration of the network is obtained by allowing the internal nodes of the network to move until the total elastic energy of the network is minimized using simulated annealing [24]. Cutting of springs, however, leads to an expansion of the hole after the equilibrium configuration of the network is obtained which results in larger and more round shapes compared to original LAA mask. In the proposed method, we will introduce two types of corrections via image processing to manipulate the size and shape of the LAA masks before cutting the spring to counteract the potential distortion of LAA following simulated annealing. The goal is to obtain a hole after finding the equilibrium configuration that is similar in size and shape to the original LAA. The naïve mapping and the optimized mapping will be applied to test images as well as real LAAs from CT images.

The complete procedure of the naïve mapping consists of the following steps: create LAA masks from a lung CT scan; superimpose LAA masks with a fully connected elastic spring network and cut spring within LAAs; solve the spring network for equilibrium.

2.2 The Curvature and Size Adjusted Mapping (CSAM)

The naïve mapping method inherently expands the size of original LAA due to the energy stored in the pre-stressed spring network. Therefore, we propose a Curvature and Size Adjusted Mapping which preprocess the LAA masks to reduce the distortion caused in the naïve mapping. The preprocessing incorporates adjustment in size and shape. The preprocessing is based on manipulation of the boundary of the LAA mask, which can be expressed as a closed curve:

$$\hat{\boldsymbol{r}}(t) = (X(t), Y(t))$$

Where $\hat{\boldsymbol{r}}(t)$ is a parametric vector that points to the boundary of a LAA mask; $X(t)$ and $Y(t)$ are the x and y coordinates of $\hat{\boldsymbol{r}}(t)$ along two orthogonal base vectors; t is a parameter ranging between 0 and 1 that describes the relative position along the boundary of LAA cluster with respect to an arbitrary starting point at t = 0.

To manipulate the size of a LAA, resize the boundary as:

$$\hat{\boldsymbol{r}}_{\boldsymbol{S}}(t) = \sqrt{\alpha} \cdot \hat{\boldsymbol{r}}(t) + (1 - \sqrt{\alpha}) \cdot \int_{t=0}^{1} \hat{\boldsymbol{r}}(t)\, dt$$

Where α is the ratio of corrected LAA size to the original size.

When $\alpha = 1$,

$$\hat{\boldsymbol{r}}_{\boldsymbol{S}}(t) = 1 \cdot \hat{\boldsymbol{r}}(t) + 0 \cdot \int_{t=0}^{1} \hat{\boldsymbol{r}}(t)\, dt = \hat{\boldsymbol{r}}(t)$$

Hence, no change is made on the corrected LAA boundary.

When $\alpha = 0$,

$$\hat{\boldsymbol{r}}_{\boldsymbol{S}}(t) = 0 \cdot \hat{\boldsymbol{r}}(t) + 1 \cdot \int_{t=0}^{1} \hat{\boldsymbol{r}}(t)\, dt = constant$$

The boundary becomes a single point of the centroid.

To manipulate the shape of a LAA, we calculate the curvature along the LAA boundary, decrease the curvature everywhere by a constant, and then reconstruct a LAA from the adjusted curvature profile:

The curvature is calculated with:

$$k(t) = \frac{\left|\left|\hat{\boldsymbol{T}}'(t)\right|\right|}{||\hat{\boldsymbol{r}}_s{}'(t)||} \tag{1}$$

Where $\hat{\boldsymbol{T}}(t)$ is the unit tangent vector of $\hat{\boldsymbol{r}}_{\boldsymbol{s}}(t)$. In another word, the curvature is calculated as the norm of the first derivative of $\hat{\boldsymbol{T}}(t)$ divided by the norm of the first derivative of $\hat{\boldsymbol{r}}_{\boldsymbol{s}}(t)$.

$\widehat{\boldsymbol{r}_{\boldsymbol{s}}'}(t)$ is calculated with either forward difference approximation or backward difference approximation.

Forward difference approximation: $\widehat{\boldsymbol{r}'}(t_i) = \widehat{\boldsymbol{D}}_+(t) = \frac{\hat{\boldsymbol{r}}(t+\Delta) - \hat{\boldsymbol{r}}(t)}{\Delta}$ (2)

Backward difference approximation: $\hat{\boldsymbol{r}}'(t) = \widehat{\boldsymbol{D}}_-(t) = \frac{\hat{\boldsymbol{r}}(t) - \hat{\boldsymbol{r}}(t-\Delta)}{\Delta}$ (3)

$T'(t)$ is obtained using a numerical approximation of the second derivative of $r_s(t)$.

$$\widehat{\boldsymbol{T}}'(t) = \frac{\frac{\widehat{\boldsymbol{D}}_+(t) - \widehat{\boldsymbol{D}}_-(t)}{t}}{||r_s{}'(t)||} \tag{4}$$

Where $||\hat{\boldsymbol{r}}_s{}'(t)||$ accounts for the unit length of $\widehat{\boldsymbol{T}}(t)$.

A constant β is subtracted from $k(t)$ to form $k_{new}(t)$:

$$k_{new(t)} = k(t) - \beta \tag{5}$$

To reconstruct $X_{new}(t)$ and $Y_{new}(t)$from $k_{new}(t)$, we integrate $k_{new}(t)$ twice with respect to t:

$$\theta(t) + \theta_0 = \int k_{new}(t)dt \tag{6}$$

$$X_{new}(t) = \int -\cos\big(\theta(t)\big)\, dt \tag{7}$$

$$Y_{new}(t) = \int \sin\big(\theta(t)\big)\, dt \tag{8}$$

θ_0 can be determined by brute force method, allowing the reconstructed boundary to have the same rotational orientation as the original boundary.

Therefore, the boundary after both size and shape adjustment can be expressed as:

$$r_{cs}(t) = (X_{new}(t), Y_{new}(t))$$

The complete procedure of the CSAM is as follows: create LAA masks from a lung CT scan; preprocess LAA masks with certain value of α and β; superimpose the preprocessed LAA masks on a fully connected elastic spring network and cut spring within LAAs; solve the spring network for equilibrium.

2.3 Evaluate Single-LAA Mapping

The mapping of a single LAA to a spring network creates corresponding rupture of springs, and the LAA in the spring network is represented by the hole created by the removal of springs. The error between the original LAA and the reconstructed LAA is defined as the morphological difference between LAA in a CT and LAA in a spring network.

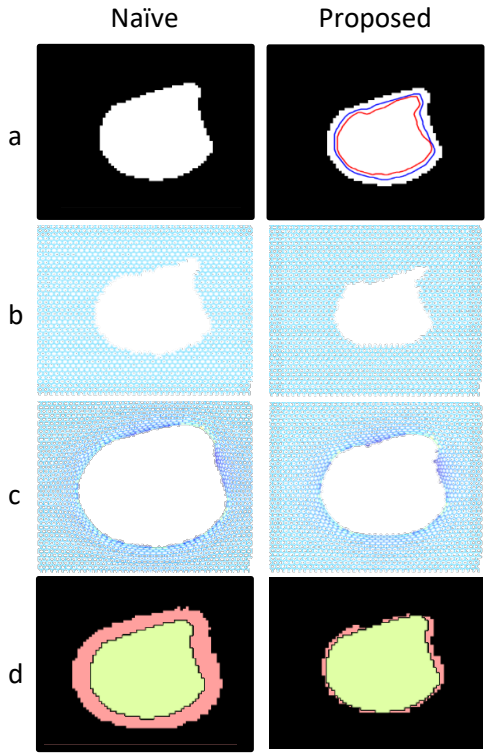

Figure 1. Mapping an Artificial LAA Map to Spring Network. (a): an artificial LAA map. In proposed mapping column, the blue boundary represents the outcome from size adjustment, and the red boundary represents that from size and shape adjustment. (b): Springs eliminated in the region corresponding to LAA. (c): the configuration equivalent to the lowest elastic energy. (d): red region highlights the reconstructed LAA map from the solved spring networks; green region is the reference to the original LAA map.

The evaluation process includes (1) constructing an apparent CT image from the spring network by converting the average spring stiffness of neighboring springs to the density of a pixel [16] and (2) evaluating the morphological difference between LAA in the

original CT and LAA in the reconstructed CT using average symmetric surface distance (ASSD), which is a common metric to evaluate segmentation quality in CT and MRI research [17]. In Figure 1, the evaluation of LAAs happens between the green and red shapes in (d). Figure 2 illustrates the calculation of ASSD of two boundaries in different colors. The main advantage of ASSD over some other metrics, like total area overlap, is that ASSD is sensitive to dissimilarities in shapes, not just sizes.

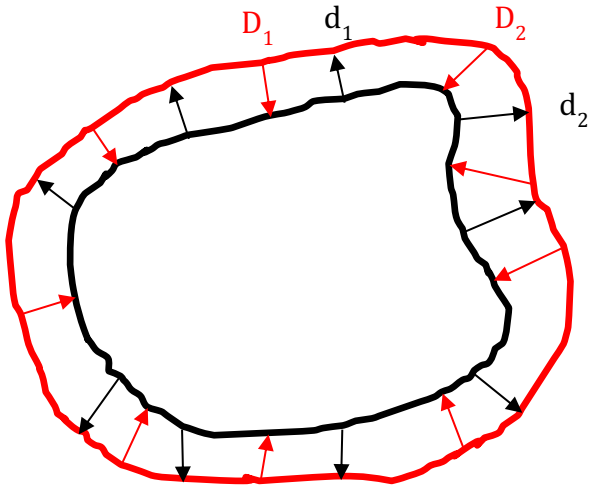

$$E_{ASSD} = \frac{1}{2N}\left(\sum_{i=1}^{N} D_i + \sum_{i=1}^{N} d_i\right)$$

Figure 2. Average Symmetric Surface Distance. The error between two boundaries in different colors is calculated as the average of closest distances from one boundary to the other.

2.4 Tuning for optimal α and β

We will test both the naïve mapping and the CSAM in a simplified scenario, in which an artificial CT with a single LAA is created and mapped into spring networks.

Considering that the time required to solve a diluted spring network for equilibrium increases nearly linearly with number of springs, we decided to set the size of

artificial CT to be smaller compared to a real CT scan. The artificial CT is initialized as a 100-pixel by 100-pixel image whose boundary pixels have density equal to 0 HU, and the majority of the area inside is set to be normal lung tissue, whose density is between -950 HU to -720 HU. A LAA was also created with density smaller than -950 HU, and the shape and size of the LAA was taken from real emphysematous lung CT.

The parameter α determines the size of the optimized LAA mask, while the parameter β determines the boundary curvature. The parameter α has theoretical values between 0 and 1. To minimize the risk of failure of reconstruction from curvature, the parameter β was limited to a conservative range [0, 0.3]. For a given artificial CT image, the LAA mask is preprocessed with all possible combination of α and β**,** with the step size for both α and β set to be 0.02. The LAA masks preprocessed with different parameters are mapped and evaluated independently in the spring networks. A matrix of error was obtained by comparing the ground truth LAA with mapped LAA from all combinations of the parameters. For each specific LAA size, the process is repeated 5 times with 5 different shapes of single LAAs cropped from an emphysematous lung CT image. The proposed mapping of 5 artificial CT images leads to 5 error maps, the parameters corresponding to the lowest error in the average of 5 error maps is considered as the optimal parameters for LAA cluster at the predefined size.

2.5 Mapping a Patient CT

After determining the values of optimal parameters, we applied both naïve method and CSAM to construct spring networks based on 20 lung CT images of

emphysema patients from National Lung Screening Trial (NLST) database. Multiple LAA clusters can exist in a patient CT scan, and CSAM was applied to preprocess every LAA individually. We used %LAA as the main metric, which was calculated by the ratio between the total LAA area and the total lung area in a CT scan. %LAA has been widely used as an indicator for the severity of emphysema. The main outcome was the %LAA measured in the ground truth CT images and the apparent CT images reconstructed from the spring networks. Specifically, we were interested in the difference of %LAA between the apparent images and the ground truth.

2.6 Model Simulation of the Progression of Emphysema

The progression of emphysema was simulated by iterative removal of springs bearing the highest forces in a network. The lung CT image of an emphysema patient was mapped into spring networks with both methods and those spring networks were progressively degraded following the same rules. Specifically, springs bearing a force that was higher than 80% of the maximum force were removed from the network at each iteration, and the configuration equivalent to the lowest elastic energy was obtained before the next iteration [3]. 30 Iterations were repeated for each spring network, and 3 measurements were collected at every iteration: the size of the largest LAA cluster, the total %LAA, and the local difference of LAA clusters between networks mapped through different methods.

The local difference of LAA clusters was quantified between two apparent CT images converted from spring networks mapped through different methods. The apparent images were partitioned into grids of 10 pixels by 10 pixels, and the $\%LAA$ of each grid

was calculated as $\%LAA_i$. The local difference was defined as the average absolute difference of $\%LAA_i$ between two images, mathematically:

$$\text{Local difference} = \frac{1}{N} \sum_{i=1}^{N} |\%LAA_{i_{naive}} - \%LAA_{i_{proposed}}|$$

Where N is the total number of grids in one image, excluding the ones without any LAA cluster in both images. The local difference was measured between two apparent CT images mapped from different methods but with similar $\%LAA$, quantifying the divergence of disease development at similar disease stage.

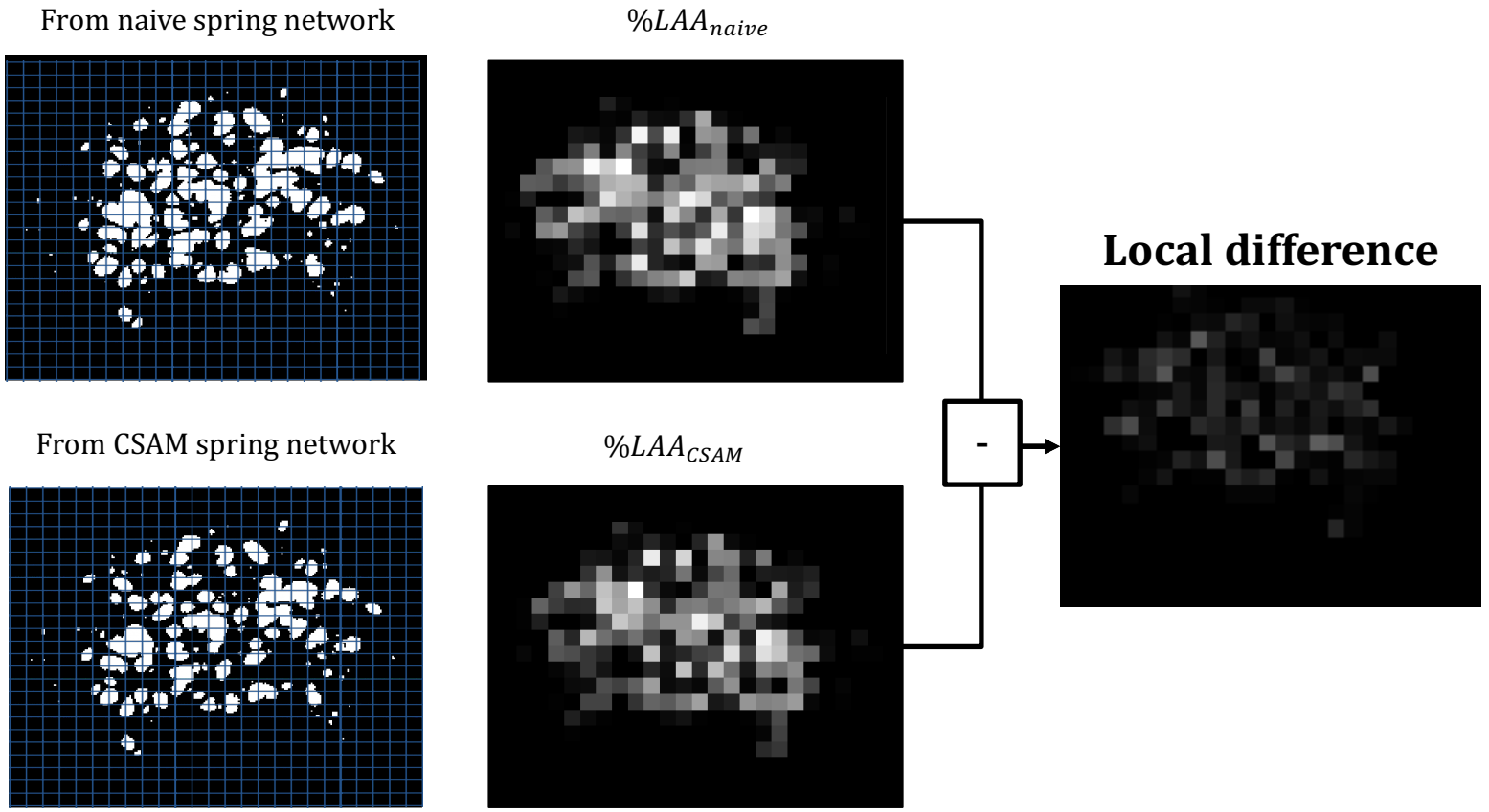

Figure 3. The Calculation of Local Difference. The apparent CT images reconstructed from spring networks of different mapping methods are partitioned into grids of interest (the left column) and the ratio of area occupied by LAA is calculated at each grid (the middle column). The absolute difference of grids at the same location is measured, and the local difference is the average absolute differences.

3 RESULTS

3.1 Mapping a Single LAA

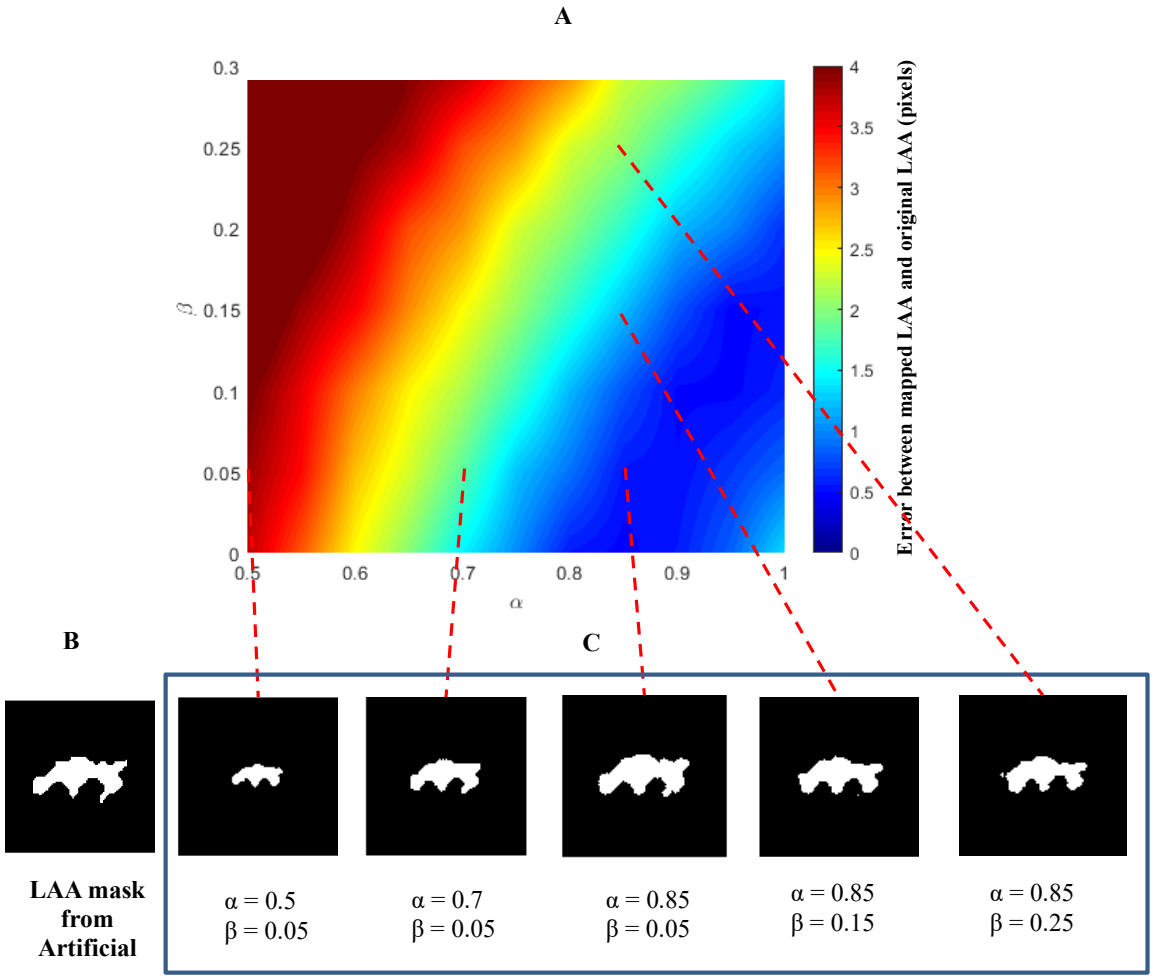

Figure 4. The Error Map of Different Parameter Combination. (A): The error map obtained by mapping an artificial single LAA map into spring networks with various combination of parameters in proposed mapping method. The error was measured between the original LAA and the reconstructed LAA image from the spring network. (B) The original LAA map. (C): Some examples of mapped LAA, which were mapped with different parameters α and β.

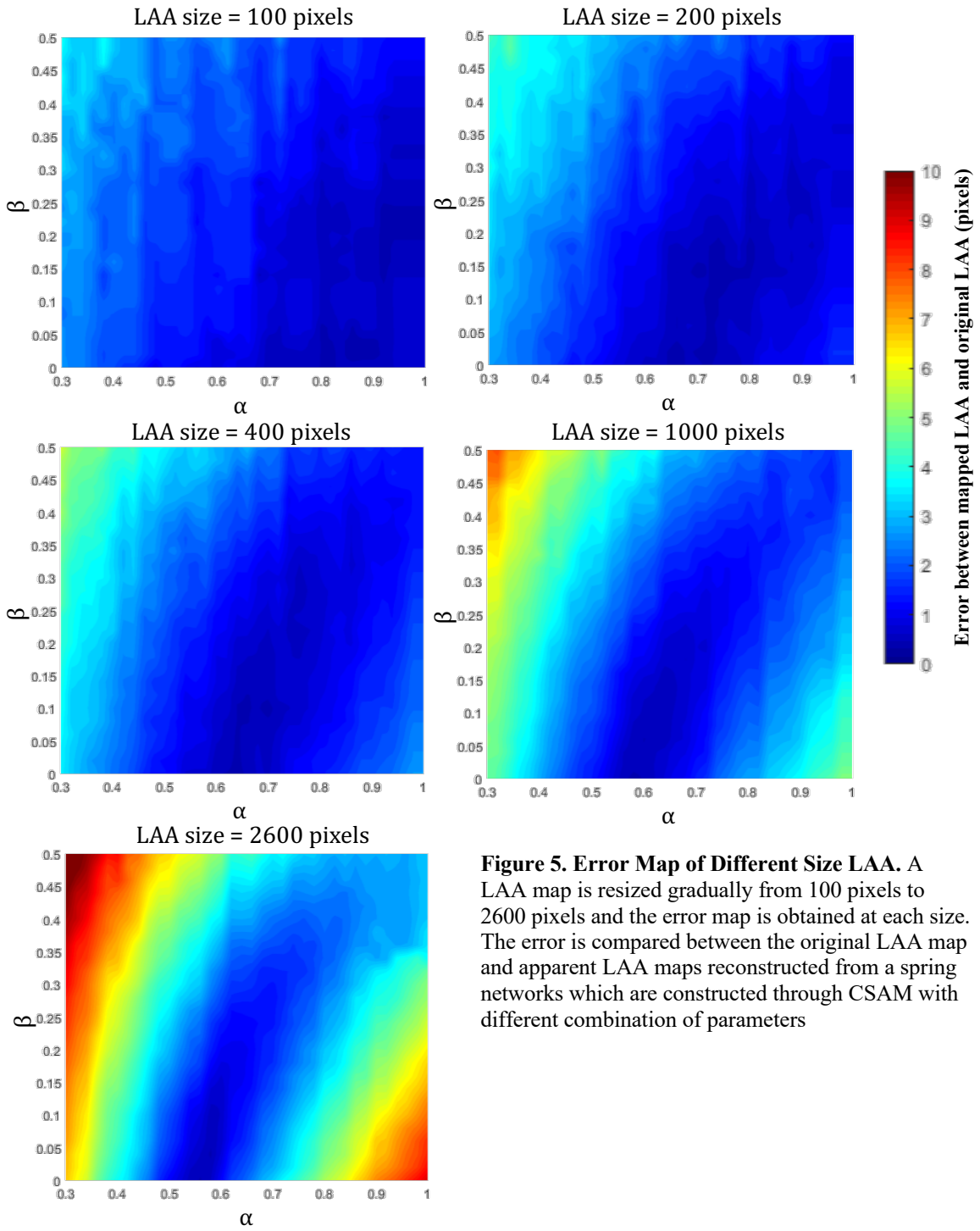

Figure 5. Error Map of Different Size LAA. A LAA map is resized gradually from 100 pixels to 2600 pixels and the error map is obtained at each size. The error is compared between the original LAA map and apparent LAA maps reconstructed from a spring networks which are constructed through CSAM with different combination of parameters

Figure 4 represents the error map obtained by performing CSAM on an artificial LAA map with different combination of parameters. Panel B represents the original LAA map and panel C represents the outcomes from spring networks constructed with different parameter combinations during the mapping process. Panel A displays the error between the original LAA (B) and the LAA in reconstructed spring network (C).

Figure 5 displays the error map of the same LAA map in different LAA sizes. As the LAA size increases from 100 pixels to 2600 pixels, the region with small errors (dark blue) gradually shrinks from almost the entire error map to a narrow valley. Furthermore, the location of the lowest error (the darkest blue) is gradually moving from the right half panel to the left panel.

Figure 6 represents the correlation between the optimal parameters, which are the parameters targeting the lowest errors in Figure 5, and the LAA sizes. The only thing different from the previous error maps is that the optimal parameters are identified within the average error map of 5 LAA in different shapes. Figure 6 displays the highly correlated relationship between the optimal α and LAA sizes with $R^2 = 0.97$, and a weaker correlation between optimal β and LAA sizes, which has $R^2 = 0.69$. Despite the strong correlation between the optimal α and LAA sizes, the variance of the optimal α at small LAA size is quite large initially and gradually decreases to a low level at large LAA size. A similar trend is found for the optimal β, which has large variance initially at small LAA size and the variance gradually diminishes as the LAA increases.

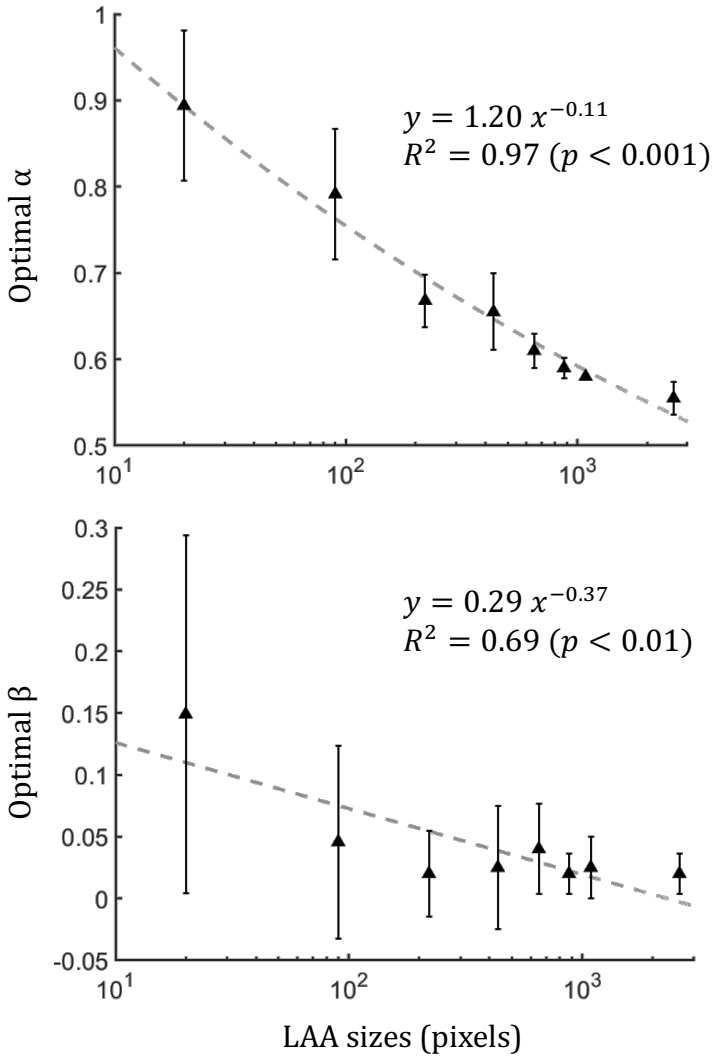

Figure 6. The Correlation between Optimal Parameters and LAA Sizes. The optimal parameters correspond to the lowest error in the error maps at different sizes.

3.2 Mapping LAA from CT Images to Spring Networks

The characteristic features of emphysema progression in CT images are represented by a set of widely varying LAA clusters, which are regions of lung tissue where mechanical failure occurred during the progression of the disease. The corresponding representation of LAA in a spring network is the void induced by the elimination of springs. Figure 7 displays a lung CT image of an emphysema patient and the spring networks carrying LAA clusters mapped with naïve and proposed method. Even though the difference between the two spring networks is hardly visible (top row), the LAA clusters mapped with the naïve method expanded out of the ground truth boundary (visualized as red lines) at single cluster level as shown in the zoomed in LAA maps (the lower row). In contrast, the CSAM method remained confined to within the original boundaries of LAA clusters with much smaller error compared to the naïve method.

20 lung CT images were obtained from the NLST database on which mapping experiments were performed both with the naïve and the CSAM methods, and the difference in $\%LAA$ was compared between the mapped spring networks and the ground truth CT images. In the case of the naïve method, the difference of $\%LAA$ increased linearly with the total $\%LAA$ in the ground truth images, with a slope of 0.27, $R^2 = 0.83$ and $p < 0.001$, indicating that the slope was significantly different from 0 (represented as a red line in Figure 7) and therefore the naïve method is undoubtedly producing systematic errors in the mapped spring networks compared to the CT images.

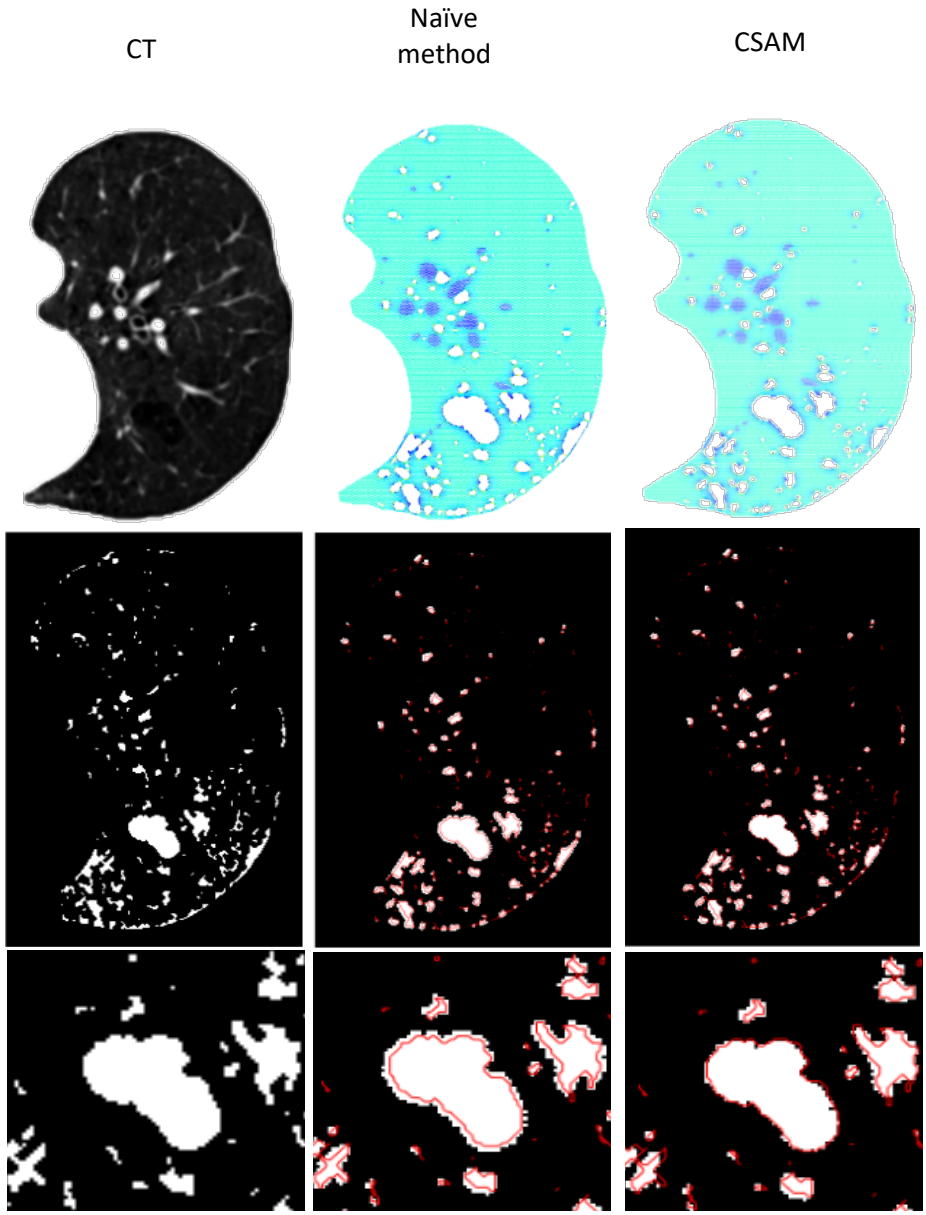

Figure 7. Mapping of LAAs from a patient CT image to spring networks. The left column displays in the order: a lung CT scan of an emphysema patient, the binary LAA map obtained by emphasizing the region < -960 HU, and a zoomed-in region of the LAA map. The middle and right columns represent the same content for two spring networks constructed from the CT images but with different mapping methods. The red boundaries represent the boundaries of LAA clusters in the left column, which serve as a reference to the ground truth.

When the mapping was conducted with the CSAM method, the slope of the regression line was not different from 0 (dashed line with p = 0.349). The overall statistics of

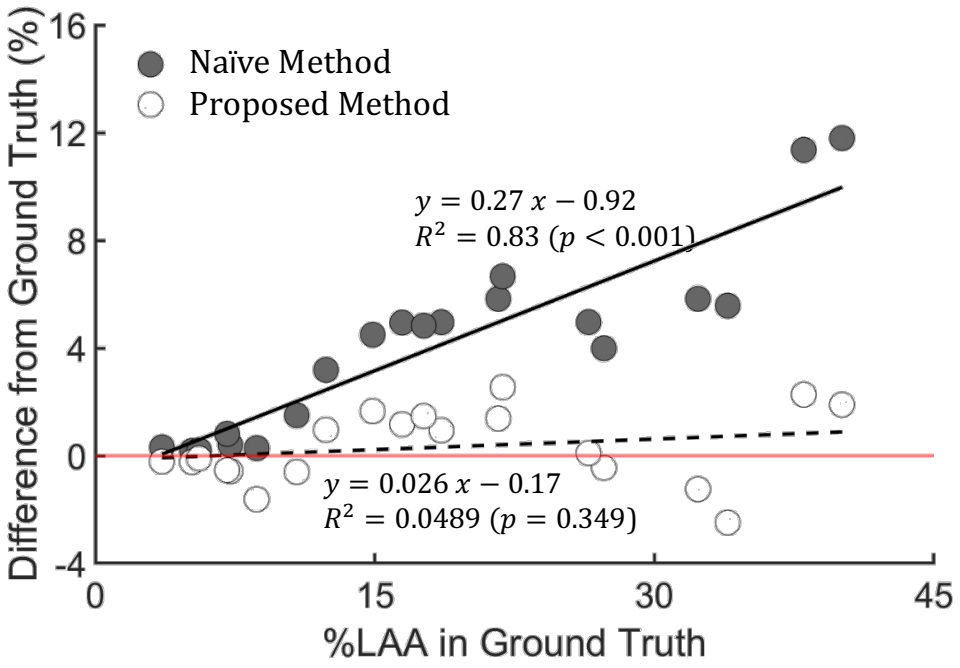

Figure 8. The Change in %LAA from CT to Spring Networks. Lung CT images with different total %LAA level were mapped into spring networks with naïve method (dark circles) and proposed method (white circles), and the difference in %LAA between the original CT images and the reconstructed spring networks were displayed in the y axis. The solid black line is the regression line to the dark circles and the dashed line is the regression line to the white circles. The transparent red line is a reference to 0.

absolute difference in %LAA is displayed as a box plot in Figure 9, and a paired t-test found a significant difference between the naïve method and the CSAM method ($p < 0.001$). Additionally, the data corresponding to CSAM method displays a much smaller variance and closer to 0 median compared to naïve method, indicating that the former reconstructs LAAs in spring networks with smaller error, better conserving the size and shape of the original LAA.

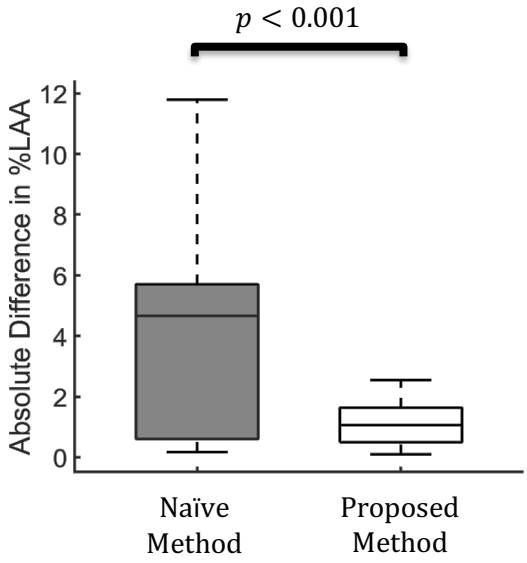

Figure 9. The Absolute Change in %LAA from CT to Spring Networks. Comparing the distribution of absolute change in %LAA between patient CTs and corresponding spring networks, the difference is significantly higher in the group of naïve method than in the group of proposed method.

3.3 Model Simulation of the Progression of Emphysema

Figure 10 shows the progressive degradation of spring networks mapped using the naïve and the CSAM methods. The springs are colored in the spectral order (blue to red) to display the increasing forces. At the initial steps, despite the LAA clusters (represented by the void regions) appearing similar across networks mapped with the two methods, the springs bearing the highest forces are not the same. As the degradation progresses, the coalescence of LAAs follows distinct orders and the morphological difference of LAA clusters eventually becomes visually distinguishable between the networks. For example, the red and black circles highlight the coalescence of specific LAA clusters in one spring network but not in the other, and such patterns take place progressively during the iterations.

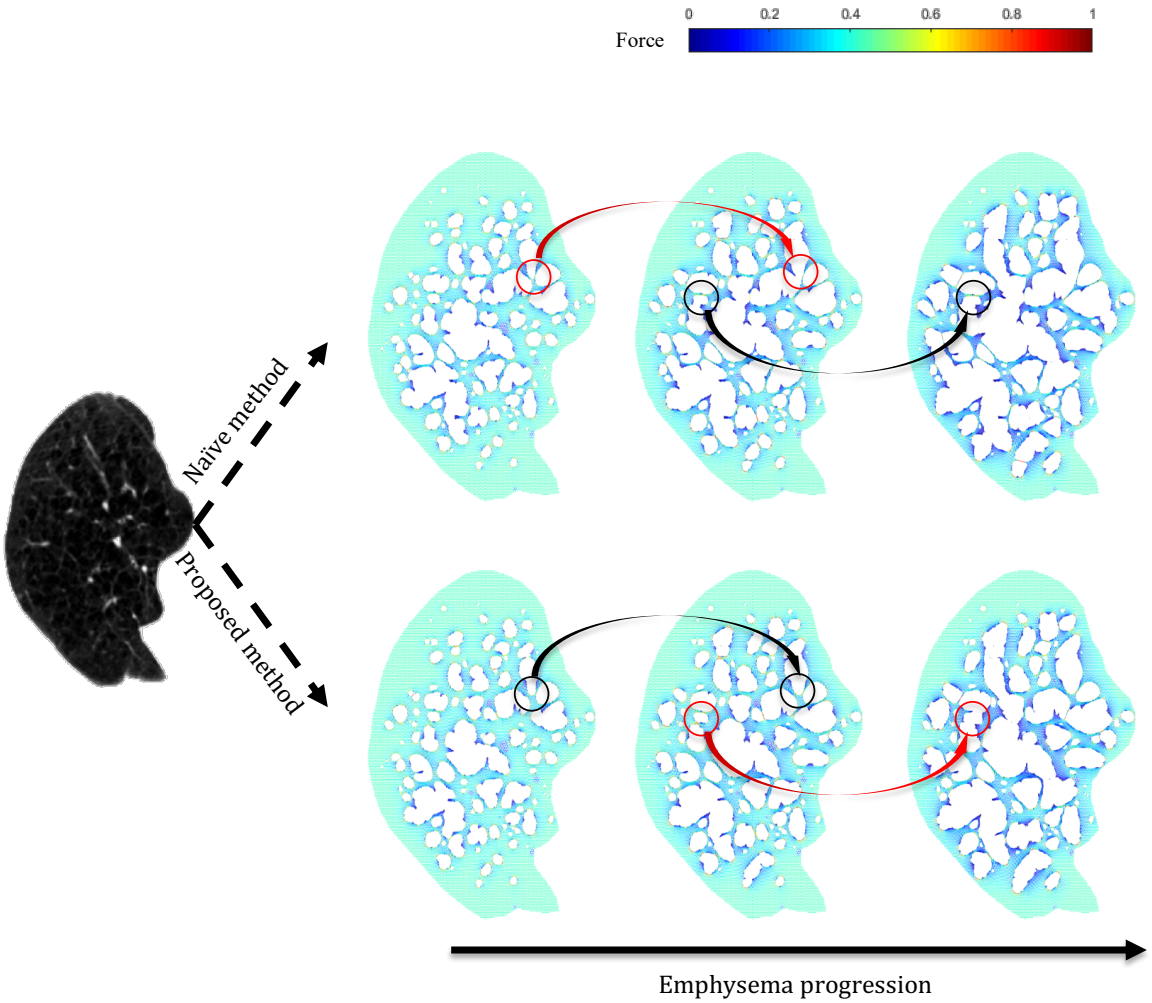

Figure 10. Imitation of the progression of emphysema. Spring networks constructed from emphysema patient lung CT images were progressive degrading with the elimination of springs to imitate the tissue destruction caused by emphysema. The red circles highlight the coalescence of LAA in one spring network but separation at the same location in another spring network (black circle).

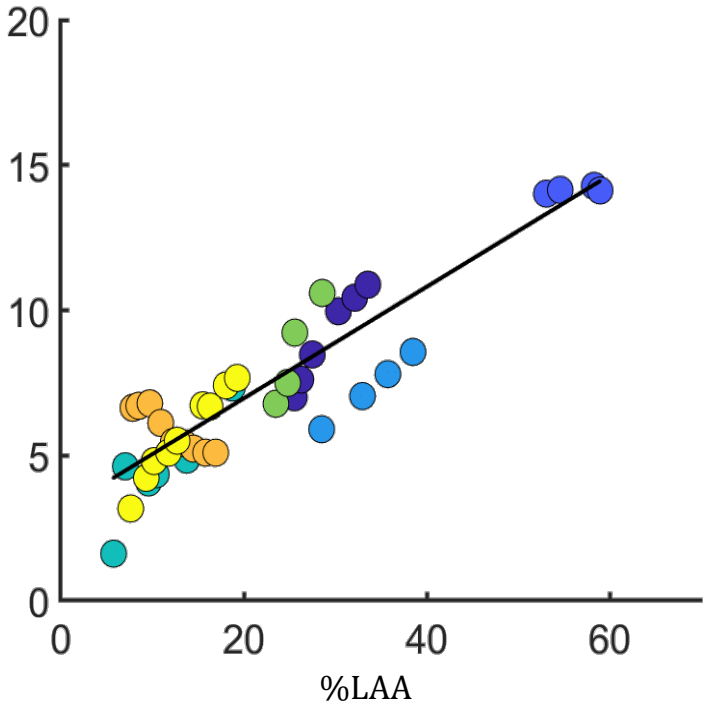

Figure 11. Divergence between Spring networks during Iterative Degradation. 7 CT images were reconstructed as spring networks (corresponding to 7 colors in the figure) with both naïve and proposed mapping methods, and all networks underwent iterative degradation to imitate the progression of emphysema. The local difference between networks mapped with different methods were measured when both networks degraded to similar pathological state (%LAA). The local difference between networks reconstructed from different methods tends to increase along with the disease severity

Figure 11 displays the morphological difference of LAA clusters across spring networks by measuring the average local difference of LAA clusters at similar %LAA, which represents similar disease severity. The color of data points denotes different subjects. Collectively, the local difference is strongly correlated with %LAA, $p = 0.91$; at single subject level, 5 out 7 subjects are strongly correlated with %LAA, $p > 0.9$, 1 subject is positively correlated with %LAA, $p = 0.68$, and 1 subject is negatively correlated with %LAA, $\rho = -0.95$. The largest LAA cluster was traced through iterations for one subject in Figure 12. The sudden increase in the size of the largest cluster implies

its coalescence with the neighboring clusters. The interesting outcome here is that the coalescence of LAA clusters may take place at different iteration with different amount of pixels for different mapping methods, consistent with the visualization in the top half of Figure 12. Until iteration 20, the absolute difference in value between the largest LAA clusters is small but nonzero. Although the largest LAA in naïve method group is initially larger than the same cluster in the CSAM method, eventually, the naïve method produces a much larger cluster at the end of the simulations. These results reveal the distinct coalescence of clusters corresponding to the two methods.

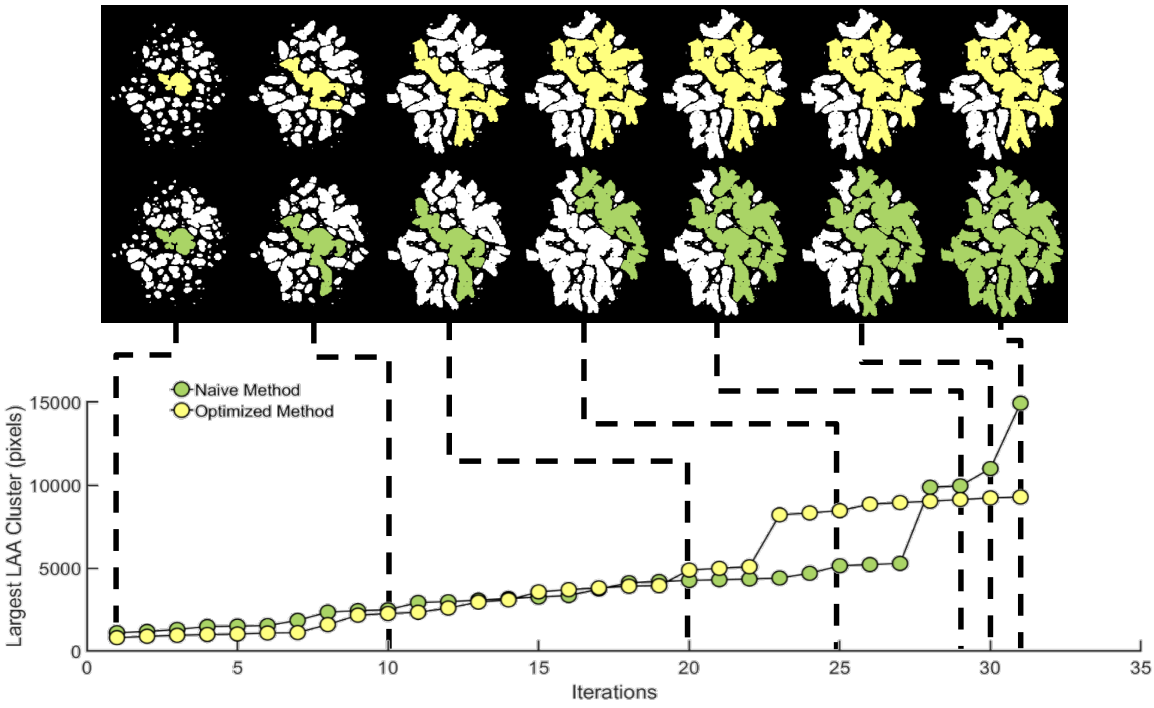

Figure 12. Largest LAA Cluster Traced in Spring Networks Constructed with Different Methods. After being reconstructed from a CT image, two spring networks underwent iterative degradation to imitate the progression of emphysema, and their largest LAA clusters were traced both visually (upper figure) and quantitatively (lower plot). Even when the largest clusters occupy similar amount of pixels (at iteration 1, 10 and 20), their morphological difference, caused by distinct coalescence of LAA clusters, can be large and visually distinguishable.

4 DISCUSSION

4.1 The Mapping Method

We have developed a novel mapping method, CSAM, in which an LAA map is preprocessed first and then a pre-stressed hexagonal elastic spring network is constructed with springs eliminated at the LAA location. The spring network is converted to an apparent CT image and compared to the original LAA map, and the error is calculated with ASSD. The error map in Figure 4 displays the responding of error to the change of parameters in CSAM. Figure 4 indicates that the error between the original LAA and the mapped LAA can be small (< 1 pixel) but not 0. The inevitable error could potentially arise from the nature of spring network and the technique discrepancy. The pre-stressed nature of spring networks prevents certain LAA shapes to be reconstructed, and the most intuitive example is a narrow rod like LAA, which is always likely to be reconstructed into a football like shape as the pre-stress expands the cut springs. Another source of error is the conversion from spring network to apparent CT images. The conversion process is equivalent to smooth the spring stiffness in a small region and the regions whose average spring stiffness is smaller than a threshold are annotated as a LAA pixel. The slight change in the threshold can significantly change the LAA shape of apparent images, hence affect the error.

The error maps look drastically different for different LAA sizes in Figure 5. The shrinking of the small error region (blue) in large LAA size suggests that a big LAA cluster is sensitive to the change of parameters when CSAM is applied, therefore the mapping of a large LAA cluster requires appropriate choice of parameter to avoid large

error in constructed spring networks. The most optimal parameters are targeting the lowest error in an error map, and the value of the optimal parameters is changing along with the LAA sizes. Figure 6 displays the strong correlation between optimal α and LAA sizes, suggesting that a larger LAA requires large adjustment in size to construct a similar spring network representation. The result is intuitive given that the elimination of more springs will result in a more expanded void region in the network. The small variance of optimal α indicates the universality of parameter α at large LAA size, that is, the parameter can be applied to different shapes of LAA without introducing large error. The parameter β displays a weaker correlation with LAA sizes and a higher variance across the spectrum of LAA size, indicating that the optimal β is sensitive to different LAA shapes and can hardly be generalized to an equation against LAA sizes.

4.2 The Mapping of Patient CT images

Figure 7 qualitatively represents the smaller error of proposed mapping method by highlighting the matching of boundary between ground truth LAA and mapped LAA, which is consistent with the smaller variance of error displayed in figure 9. However, it should be noted that some small LAA clusters exhibit similar morphology after being mapped onto the spring network with different methods. In other words, the result of the CSAM mapping is equivalent to that of the naïve mapping when the target is a small LAA cluster. Potential reasons are: (1) the size and shape adjustment are too small to alter the original morphology of the LAA cluster. (2) the resolution of the spring network is so coarse that small change in the LAA map is not reflected in the spring network. The

size and shape adjustments become negligible only when the target LAA has an extremely small size (fewer than 20 pixels) within which the expansion of area due to eliminating of springs is limited. Thus, it is reasonable to apply the naïve mapping on such clusters based on previous findings that the coalescence of LAA clusters is much more likely to occur near advanced emphysematous regions involving large LAA clusters. [25] Therefore, the small clusters away from large ones will have limited contribution to the progression of emphysema, and the ones close enough to advance emphysematous regions are more likely to merge into the neighboring clusters. Neither case will negatively affect the spring network representation of the LAAs. The issue of coarse spring network resolution may produce errors based on a previous study which found that small ratio of spring network resolution to CT resolution can lead to significant underestimation of LAA size in the reconstructed apparent CT images. [26] The underestimation of a single LAA may not be vital, but the underestimation of two nearby LAA clusters may alleviate the local pathological state by separating two LAA clusters further apart. As a limitation of this thesis, the spring network resolution was not fine enough to avoid such issue, which may be partly responsible for the negative errors (maybe even the highest error) in Figure 8.

In Figure 8, the correlation between error and total %LAA in the naïve method group is lost in the CSAM method group, suggesting that the size of LAA clusters is correctly conserved in the spring network representation during the CSAM mapping. Despite the lack of previous studies in a similar topic, the loss of correlation and the significantly smaller error in CSAM group (Figure 9) suggest that the proposed mapping

method successfully improved over the distorting effects of the naïve mapping method.

The pre-stress was assumed to be a constant through the entire study, but the value of pre-stress that reflects accurate physiological characteristic of a lung has not been determined. Since the spring network model was simplified to be linearly elastic and all springs were pre-set with the same spring constant, the amount of pre-stress was determined by the ratio between the initial length ($L_{initial}$) and the rest length (L_{rest}) of the springs.

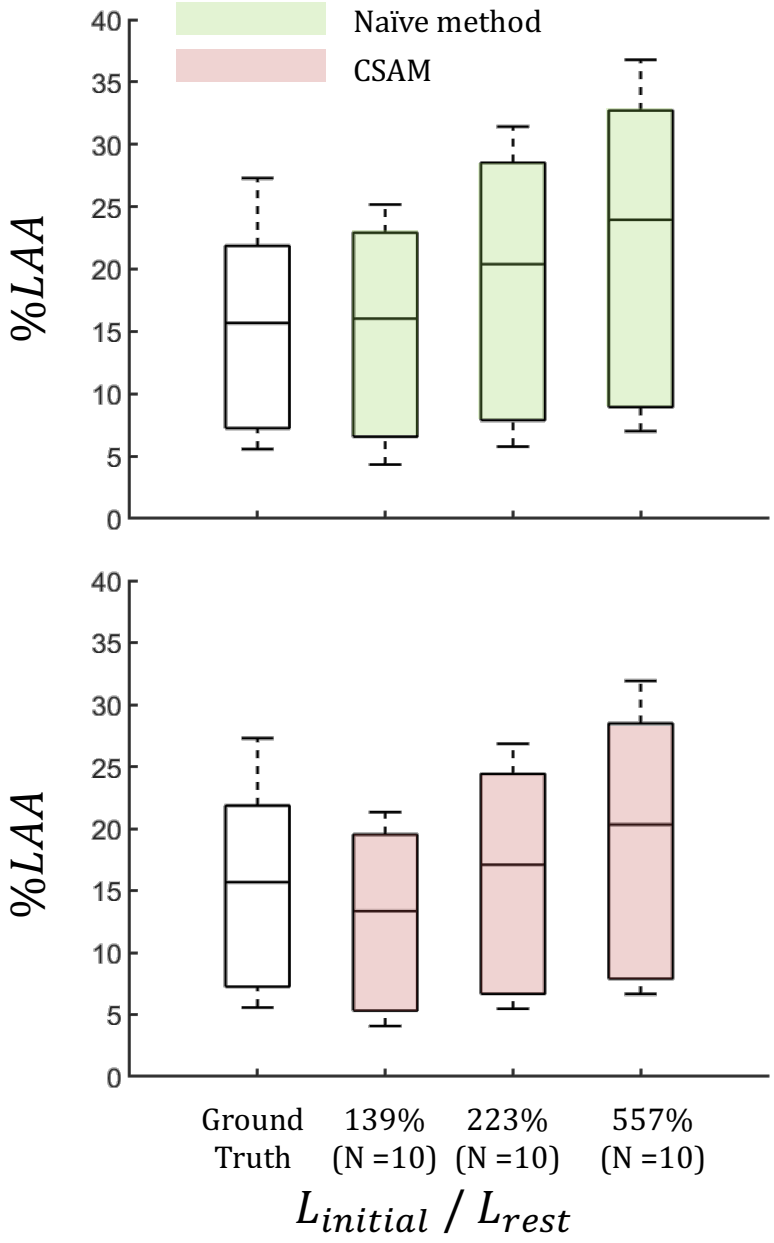

Figure 13. The impact of pre-stress on elastic spring network model. All springs are linearly elastic, hence the ratio of initial length to the rest length of springs determines the magnitude of the pre-stress. In both naïve and CSAM groups, total %LAA of constructed spring networks increases along with the amount of pre-stress.

Spring networks were constructed from the same set of CT subjects with different pre-stress, and the total %LAA were measured at corresponding apparent CT Images. Figure

13 demonstrates the impact of pre-stress on our spring network model by presenting the distribution of total %LAA at different pre-stress setting. Higher pre-stress results in higher total %LAA in all 10 subjects with both naïve method ($\rho = 0.93$) and CSAM ($\rho = 0.93$). The result is intuitive with the fact that a fully connected spring network with higher pre-stress is bearing higher energy at each spring, hence cutting the same amount of springs will result in a larger void area. The result also implies that the optimal parameters of CSAM is related to the pre-stress, therefore the ideal range of pre-stress that reflects actual lung physiology should be identified to determine the optimal parameters of CSAM with clinical potential.

4.3 Model Simulation of Emphysema Progression

The proposed CSAM mapping method constructs spring network representations of emphysematous lung with better conservation to the original CT image than the naïve method. However, the qualitative difference between the network representations is subtle despite the significant difference in quantitative analysis. Thus, it is reasonable to test the necessity of proposed method by measuring the long-term difference between the naïve and proposed methods during the simulation of emphysema progression.

Despite the similarities between the LAA configurations of the two methods at the initial iteration, Figure 10 shows qualitative differences demonstrated by the different force distribution profile across spring networks which manifest in the distinct LAA coalescence dynamic at later stages of the progression. The different location of coalescence between the two methods indicates that the redistribution of force after spring rupture follows distinct profiles, and the progressive iterations of such process

drives the accumulation of divergence between the networks corresponding to the two different mapping methods, ultimately resulting in completely distinct LAA configurations. However, the LAA structures in Figure 10 look somewhat similar even at an advanced disease stage. A possible reason is that the criteria for removing springs at each iteration, the springs bearing more than 80% of the maximum force, is too broad and there exists a great overlap of springs bearing the highest forces across the spring networks. A finer step size of removing springs requires higher computational resource but may reveal more obvious divergence between the spring networks of different groups in long term simulation of emphysema progression.

Figure 11 quantitatively represents the divergence between spring networks by measuring the average local difference at similar disease severity. The globally strong correlation between local difference and disease severity demonstrates a collective behavior of increasing divergence between the two spring networks as emphysema progresses, consistent with previous discussion about the accumulating divergence due to redistribution of force after springs rupture at distinct location. A similar phenomenon is shown in Figure 12, where the largest LAA clusters coalesce with neighboring clusters at different order in two groups of spring networks. At the level of a single subject (specific colored data points in figure 11), 6 out of 7 followed global behavior and exhibit strong correlation between local difference and pathological state, while only 1 subject behaved conversely. The specific subject is examined in more detail in Figure 14.

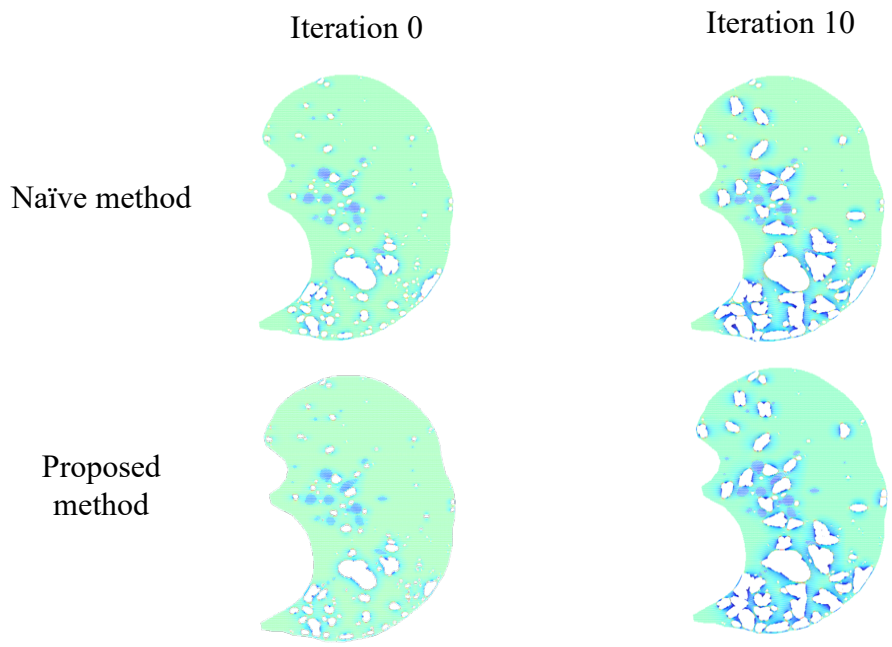

Figure 14. The Exception. The only spring network exhibits decreasing local difference along with disease severity.

Based on visual assessment, there may be two reasons that can account for the decreasing local difference: (1) the structure includes many tiny LAA clusters, and (2) as previously mentioned, the coarse criteria of removing springs at each iteration. Despite the existence of a single large LAA cluster, the majority of LAA clusters are small that these clusters do not even require any preprocessing by our CSAM method. Therefore, with the contribution of coarse degrading criteria, almost identical spring networks at the initial iteration eventually progress to similar configurations.

Although the patient specific simulation of emphysema progression utilizing mechanical forces implicitly assumes that rupture sites are also related to increased local enzyme concentrations, additional factors probably contribute to tissue deterioration such as exacerbation [27], infections, smoking, and potential other co-morbidities. The

increasing difference between the prediction of progression by the two mapping methods more likely reflects more complex network effects as mechanical forces are redistributed around a rupture site.

Table 1. The impact of β on emphysema simulation.

CT 1	β = 0.1		β = 0.2	
	%LAA	#LAA	%LAA	#LAA
Iteration 0	13.34	122	11.08	115
Iteration 1	14.37	116	12.37	110
Iteration 2	16.78	113	12.96	109
Iteration 3	18.30	113	15.40	107
Iteration 4	19.04	111	16.23	100
Iteration 5	20.72	112	18.51	100
Iteration 6	22.73	106	19.35	96
Iteration 7	24.78	99	20.79	93
Iteration 8	27.01	92	21.52	92
Iteration 9	27.93	90	22.85	91
Iteration 10	30.42	89	25.18	83

CT 2	β = 0.1		β = 0.2	
	%LAA	#LAA	%LAA	#LAA
Iteration 0	19.10	105	14.86	115
Iteration 1	20.24	102	16.70	107
Iteration 2	23.96	100	17.68	104
Iteration 3	25.29	96	19.22	99
Iteration 4	27.21	94	20.71	98
Iteration 5	29.07	90	22.65	95
Iteration 6	30.32	88	24.61	93
Iteration 7	33.09	83	27.89	91
Iteration 8	36.42	84	28.56	87
Iteration 9	38.29	78	30.66	88
Iteration 10	39.74	76	33.74	84

β was the parameter that adjusts the shape of a LAA cluster in CSAM. Despite the observation that the optimal β is usually a small number, yet the relationship between the optimal β and the LAA size was not found. Thus, CSAM was implemented with a constant β = 0.05 throughout the study. However, a slight change in β may result in completely different layout of neighboring LAA clusters, e.g., a smaller β allows two LAA clusters be closer to each other, therefore they may merge with a higher probability based on the mechanical force driven theory of emphysema. To study the impact of β on the simulation of emphysema progression, four spring networks were reconstructed from two CT images with CSAM and two different parameter β, 0.1 and 0.2 respectively. Those 4 spring networks were then undergoing 10 iterations of disease progression simulation, while the ratio of area occupied by LAA clusters (%LAA) and the number of

LAA clusters (#LAA) were measure at corresponding apparent CT images at each iteration. Based on the results in table 1, the %LAA at iteration 0 always decreases as the value of β increases, suggesting that shape adjustment was implemented through the erosion of original shape. The erosion of a LAA cluster not only accompanies a smaller %LAA, but also a higher probability that one LAA cluster would be separated into two clusters if there was initially a narrow connection between them. Based on the finding in %LAA, the number of LAA clusters should be more likely to increase as a larger β is applied. The column of #LAA partially agrees with the previous finding by presenting both increased and decreased #LAA at iteration 0 for a larger β. The only explanation for a decreased #LAA is the elimination of LAA clusters under a high value of β, and Figure 15 supports the explanation by visualizing the shape adjustment of β from small to large level.

Figure 15. The Elimination of LAA at Large value β.

The simulation of emphysema progression was performed on all 4 spring networks and table 1 reveals that different β values can result in distinct progression trajectories. For example, %LAA is 20.7% and #LAA is 112 for CT1 at iteration 5 with β = 0.1, whereas similar %LAA is found at iteration 7 when β = 0.2 and #LAA is 93.

Similar %LAA but much smaller #LAA due to the use of different parameter value indicates the distinct LAA clusters profile and progression trajectories at two networks.

4.4 Limitations

Various simplifications were made during the development of the mapping methods, subsequently resulting in limitations of the analysis and the results related to disease progression.

First and foremost, the ratio of spring network resolution to CT resolution was not large enough to generate unbiased results. The coarse spring network resolution does not accurately reflect the LAA map of the original CT image and the subsequently reconstructed apparent CT is different from the original LAA map. Especially at the boundary of a LAA cluster, this phenomenon can happen with a high likelihood due to the mismatch between a CT pixel and a coarse spring network cell. An accurate boundary profile is critical when two neighboring LAA clusters are separated only by a thin wall. In this case, inaccurate representation of the cluster boundaries by the spring network can lead to an early coalesce of clusters during simulated progression of emphysema. Indeed, the progression by mechanical forces is overly sensitive to small changes in such boundaries. Therefore, the coarse network resolution may lead to a biased prediction of the emphysema progression.

Another simplification is the smoothing of LAA map before the construction of spring network representation. To reduce the strong effects of single LAA pixels or tiny LAA cluster on the reconstruction, every LAA map was initially smoothed with image

dilation and image erosion, subsequently reducing the total number of LAA clusters to a much smaller level.

Another limitation of modeling, especially that of the prediction of progression, is related to transforming the original CT image to a binary LAA map. This transformation leads to a loss of information. In the future, the non-LAA pixels may be represented by springs of different stiffness, which in turn may provide a better representation of the lung's elastic structure.

Eventually, the generic 2D nature of the network model limits the potential of investigating the complete pathological mechanism of emphysema. A recent study [23] has found a potentially novel model of emphysema progression by analyzing 3D CT data, which is unlikely to be recapitulated in 2D due to the absence of one-dimensional information. Nevertheless, our approach can be extended to 3D in the future.

5 CONCLUSION

5.1 Summary

We developed a novel method of reconstructing a pre-stressed spring network representation of emphysematous lungs through analysis of the characteristic regions, the LAAs, from emphysema patient lung CT scans. Our results suggest that the proposed method is able to construct spring network representation of emphysematous lungs while retaining a better correspondence with the original structure in the CT images than the naïve method. Therefore, our proposed CSAM method can be applied to personalize spring network models with patient specific information, subsequently helping in predicting the progression of emphysema. Our study may have implications for early intervention, and even guiding decision-making in LVRS and Bronchoscopic Lung Volume Reduction (bLVR) surgeries.

5.2 Future Work

The personalization of a finite element model should be validated by clinical data [28]. Therefore, the patient specific spring network model should be applied to make prediction about future state of emphysema with the verification of real follow-up CT images. The personalized nature of the model will allow the direct comparison of the microscopic structure between the model output and clinical obtained CT, which may allow the model to study characteristic emphysema progression mechanisms of patients with certain microscopic features. Previous studies longitudinally investigated the microscopic change in lungs of emphysema patients without microscopic mechanical simulation. [23] [25] The patient specific model can be applied to reproduce the results as

well as interpret potential difference in microscopic structure between the model and CT. The potential difference may provide insights into new factors or parameters that can be incorporated into the model to achieve higher consistency with clinical data. Using extensive simulations, patient specific model predictions can be compared with clinical obtained CT data, which may identify distinct parameters, factors and iterative criteria for different groups of emphysema patients with different pathological characteristics.

A recent lung CT analysis has led to the discovery of super large low attenuation clusters in 3D which was shown significantly contribute to emphysematous progression [23]. The extension to 3D model is a necessary next step before fully understanding the role of mechanical forces in the progression of emphysema. Identical to the case of our 2D model, the 3D model should be extensively simulated and compared with CT images to validate its efficacy in predicting the progression of emphysema. The ultimate goal is to improve the patient specific model to a stable and accurate predictor that can be applied to help guiding decision-making in surgeries like LVRS and bLVR.

BIBLIOGRAPHY

1 Tuder RM, Petrache I, Elias JA, Voelkel NF, Henson PM. (2003). Apoptosis and emphysema: the missing link. *American Journal of Respiratory Cell and Molecular Biology*. 28(5):551–554.

2 Suki, B. and Parameswaran, H. (2014). Computational modeling helps uncover mechanisms related to the progression of emphysema. *Drug Discovery Today. Disease Models.* 70:4245–4249. http://dx.doi.org/10.1016/j.ddmod.2014.03.001

3 M. Mishima, T. Hirai, H. Itoh, Y. Nakano, H. Sakai, S. Muro, et al. (1999). Complexity of terminal airspace geometry assessed by lung computed tomography in normal subjects and patients with chronic obstructive pulmonary disease. *Proceedings of the National Academy of Sciences of the United States of America*. 96:8829–8834.

4 B. Suki, K.R. Lutchen, E.P. Ingenito (2003). On the progressive nature of emphysema: roles of proteases, inflammation, and mechanical forces. *American Journal of Respiratory and Critical Care Medicine*. 168:516–521.

5 N.L. Müller, C.A. Staples, R.R. Miller, R.T. Abboud (1988). 'Density mask': an objective method to quantitate emphysema using computed tomography. *Chest,* 94(4): 782-787. Doi: 10.1378/chest.94.4.782

6 Snider GL, Lucey EC, Stone PJ. (1986). Animal models of emphysema. *American Review of Respiratory Disease*. 133:149–169.

7 Janoff AJ. (1985) Elastases and emphysema: current assessment of the protease-antiprotease hypothesis. *American Review of Respiratory Disease*. 132:417–433.

8 Hautamaki RD, Kobayashi DK, Senior RM, Shapiro SD. (1997). Requirement for macrophage elastase for cigarette smoke-induced emphysema in mice. *Science.* 277:2002–2004.

9 D'Armiento J, Dalal SS, Okada Y, Berg RA, Chada K. (1992). Collagenase expression in the lungs of transgenic mice causes pulmonary emphysema. *Cell*. 71:955–961.

10 Finlay GA, O'Driscoll LR, Russell KJ, D'Arcy EM, Masterson JB, FitzGerald MX, O'Connor CM. (1997). Matrix metalloproteinase expression and production by alveolar macrophages in emphysema. *American Journal of Respiratory and Critical Care Medicine.* 156:240–247.

11 Croxton TL, Weinmann GG, Senior RM, Wise RA, Crapo JD, Buist AS. (2003). Clinical research in chronic obstructive pulmonary disease: Needs and opportunities. *American Journal of Respiratory and Critical Care Medicine.* 167: 1142–1149.

12 Brenner M, McKenna RJ Jr, Gelb AF, Fischel RJ, Wilson AF. (1998). Rate of FEV1 change following lung volume reduction surgery. *Chest.* 113:652–659.

13 Shapiro SD, Senior RM. (1999). Matrix metalloproteinases: matrix degradation and more. *American Journal of Respiratory Cell and Molecular Biology.* 20:1100–1102.

14 Kononov S, Brewer K, Sakai H, Cavalcante FSA, Sabayanagam CR, Ingenito EP, Suki B. (2001). Roles of mechanical forces and collagen failure in the development of elastase-induced emphysema. *American Journal of Respiratory and Critical Care Medicine.* 164:1920–1926.

15 Wang, Z., Gu, S., Leader, J.K. et al. (2013). Optimal threshold in CT quantification of emphysema. *European Radiology.* 23:975–984. https://doi.org/10.1007/s00330-012-2683-z

16 Wellman, T. J., Mondoñedo, J. R., Davis, G. S., Bates, J. H. T. & Suki, B. (2018). Topographic distribution of idiopathic pulmonary fibrosis: a hybrid physics- and agent-based model. *Physiological Measurement.* 39(6):064007. https://doi.org/10.1088/1361-6579/aaca86

17 Akkus, Z., Galimzianova, A., Hoogi, A. et al. (2017). Deep Learning for Brain MRI Segmentation: State of the Art and Future Directions. *Journal of Digital Imaging*. 30:449–459. https://doi.org/10.1007/s10278-017-9983-4

18 West, J.B. (1971). Distribution of mechanical stress in the lung, a possible factor in localization of pulmonary disease." *The Lancet.* 297(7704):839–841. https://doi.org/10.1016/S0140-6736(71)91501-7

19 Takahashi, Ayuko, Arnab Majumdar, Harikrishnan Parameswaran, Erzsébet Bartolák-Suki, and Béla Suki. (2014). Proteoglycans Maintain Lung Stability in an Elastase-Treated Mouse Model of Emphysema. *American Journal of Respiratory Cell and Molecular Biology.* 51(1):26–33. https://doi.org/10.1165/rcmb.2013-0179OC

20 Mondoñedo, Jarred R., and Béla Suki. (2017). Predicting Structure-Function Relations and Survival Following Surgical and Bronchoscopic Lung Volume Reduction Treatment of Emphysema. *PLoS Computational Biology.* 13(2):e1005282. https://doi.org/10.1371/journal.pcbi.1005282

21 Little, J. Paige, and Clayton Adam. “Development of a Computer Simulation Tool for Application in Adolescent Spinal Deformity Surgery.” In *Biomedical Simulation*, edited by Fernando Bello and Stéphane Cotin, 5958:90–97. Lecture Notes in Computer Science. Berlin, Heidelberg: Springer Berlin Heidelberg, 2010. https://doi.org/10.1007/978-3-642-11615-5_10

22 Little, J. Paige, and Clayton Adam. (2011).Patient-Specific Computational Biomechanics for Simulating Adolescent Scoliosis Surgery: Predicted vs Clinical Correction for a Preliminary Series of Six Patients. *International Journal for Numerical Methods in Biomedical Engineering* 27(3):347–356. https://doi.org/10.1002/cnm.1422

23 Mondoñedo, Jarred R., Susumu Sato, Tsuyoshi Oguma, Shigeo Muro, Adam H. Sonnenberg, Dean Zeldich, Harikrishnan Parameswaran, Toyohiro Hirai, and Béla Suki. (2019). CT Imaging-Based Low-Attenuation Super Clusters in Three Dimensions and the Progression of Emphysema. *Chest* 155(1):79–87. https://doi.org/10.1016/j.chest.2018.09.014

24 Cavalcante, Francisco S. A., Satoru Ito, Kelly Brewer, Hiroaki Sakai, Adriano M. Alencar, Murilo P. Almeida, José S. Andrade, Arnab Majumdar, Edward P. Ingenito, and Béla Suki. (2005). Mechanical Interactions between Collagen and Proteoglycans: Implications for the Stability of Lung Tissue. *Journal of Applied Physiology* 98(2): 672–679. https://doi.org/10.1152/japplphysiol.00619.2004

25 Tanabe, Naoya, Shigeo Muro, Susumu Sato, Shiro Tanaka, Tsuyoshi Oguma, Hirofumi Kiyokawa, Tamaki Takahashi, et al. (2012). Longitudinal Study of Spatially

Heterogeneous Emphysema Progression in Current Smokers with Chronic Obstructive Pulmonary Disease. *PLoS ONE.* 7(9): e44993. https://doi.org/10.1371/journal.pone.0044993

26 Diciotti, Stefano, Alessandro Nobis, Stefano Ciulli, Nicholas Landini, Mario Mascalchi, Nicola Sverzellati, and Bernardo Innocenti. (2017). Development of Digital Phantoms Based on a Finite Element Model to Simulate Low-Attenuation Areas in CT Imaging for Pulmonary Emphysema Quantification. *International Journal of Computer Assisted Radiology and Surgery* 12(9):1561–1570. https://doi.org/10.1007/s11548-016-1500-6

27 Tanabe, Naoya, Shigeo Muro, Toyohiro Hirai, Tsuyoshi Oguma, Kunihiko Terada, Satoshi Marumo, Daisuke Kinose, Emiko Ogawa, Yuma Hoshino, and Michiaki Mishima. (2011). Impact of Exacerbations on Emphysema Progression in Chronic Obstructive Pulmonary Disease. *American Journal of Respiratory and Critical Care Medicine.* 183(12):1653–1659. https://doi.org/10.1164/rccm.201009-1535OC

28 Stevanella, Marco, Francesco Maffessanti, Carlo A. Conti, Emiliano Votta, Alice Arnoldi, Massimo Lombardi, Oberdan Parodi, Enrico G. Caiani, and Alberto Redaelli. (2011). Mitral Valve Patient-Specific Finite Element Modeling from Cardiac MRI: Application to an Annuloplasty Procedure. *Cardiovascular Engineering and Technology* 2(2):66–76. https://doi.org/10.1007/s13239-010-0032-4

29 Hamakawa, Hiroshi, Erzsébet Bartolák-Suki, Harikrishnan Parameswaran, Arnab Majumdar, Kenneth R. Lutchen, and Béla Suki. (2011). Structure–Function Relations in an Elastase-Induced Mouse Model of Emphysema.” *American Journal of*

Respiratory Cell and Molecular Biology 45(3):517–524.

https://doi.org/10.1165/rcmb.2010-0473OC

CURRICULUM VITAE